

Dynamics of strongly correlated fermions: *Ab initio* results for two and three dimensions

N. Schlünzen, S. Hermanns, and M. Bonitz

Institut für Theoretische Physik und Astrophysik, Christian-Albrechts-Universität zu Kiel, D-24098 Kiel, Germany

C. Verdozzi

Department of Physics and ETSF, Lund University, Box 118, S-22100 Lund, Sweden

(Received 13 August 2015; revised manuscript received 16 December 2015; published 11 January 2016)

Quantum transport of strongly correlated fermions is of central interest in condensed matter physics. While the stationary expansion dynamics have recently been measured with cold atoms in 2D optical lattices, *ab initio* simulations have been limited to 1D setups so far. Here, we present the first precise fermionic quantum dynamics simulations for 2D and 3D. The simulations are based on nonequilibrium Green functions and incorporate strong correlations via T -matrix self-energies. The simulations predict the short-time dynamics, and we discover a universal scaling of the expansion velocity with the particle number. Our predictions can be verified experimentally using the recently developed fermionic atom microscopes.

DOI: [10.1103/PhysRevB.93.035107](https://doi.org/10.1103/PhysRevB.93.035107)**I. INTRODUCTION**

Particle, momentum, and energy transport of strongly correlated quantum systems are of growing interest in condensed matter [1–3], ultracold quantum gases [4–8], and dense plasmas [9]. Direct measurements of quantum transport have been accomplished in Hubbard-type one- and two-dimensional (1D, 2D) optical lattices by monitoring the expansion of ultracold atoms following a confinement quench [4,6–8], for an illustration see Fig. 1. Also, the dynamics following a quench in lattice depth have been measured [11–14], and very recently, three groups reported the development of an atomic microscope for fermions [15–17] opening the way for experiments with unprecedented single-site resolution. In contrast to the experiment, theoretical studies of these transport processes for fermions face fundamental difficulties. While, in 1D, the expansion of fermions can be accurately simulated with time-dependent density matrix renormalization group (DMRG) methods, e.g., Refs. [5,6], currently higher dimensions are not accessible [18].

The authors of Ref. [4] also presented 2D numerical results from a semiclassical Boltzmann equation (SC-BE) model with a collision integral in the relaxation-time approximation (RTA). One important feature of the experiment—the reduction of the expansion velocity C_{exp} of the central part (the “core,” defined as half width at half maximum [HWHM]) of the density with the Hubbard coupling strength U (see Sec. II A) and, eventually, shrinkage of the core—is qualitatively captured by RTA, see lower part of Fig. 1. However, additional observations, such as the zero crossing of C_{exp} around $U = 3$ are missed, the value of C_{exp} at large $|U|$ is off by several 100%, and even the value for the ideal case ($U = 0$) is not reproduced. This is, of course, not unexpected [4] due to the known defects of the SC-BE that include the violation of total energy conservation and an incorrect asymptotic state [20,21]. Also, the experimental system is well isolated so the dynamics should be unitary (reversible), which is in contrast to the Boltzmann equation. The RTA, in addition, assumes that the system is close to local thermal equilibrium, which may be adequate only at a late stage of the expansion.

It is the purpose of this paper to present a theory that overcomes all these problems. We present the first *ab initio* quantum simulations for correlated fermions that apply not only to one-dimensional systems but also to two and three dimensions. We capture not only the final stage of hydrodynamic expansion but also the early period where the system is far from equilibrium, and correlations and entanglement emerge. The method of choice are first-principles nonequilibrium Green functions (NEGF) simulations—a theory long established in quantum statistical mechanics, e.g., Refs. [21,22]—and demonstrate that it is capable to accurately simulate correlated fermions in Hubbard lattices, in general, and fermionic atoms in optical lattices under realistic experimental conditions, in particular.

A first confirmation is shown in the lower part of Fig. 1 where we report excellent *quantitative agreement with the experiment* [4] for all U without any free parameters. Furthermore, we present extensive additional predictions of quantum dynamics not yet observed experimentally: (a) the early stage of the evolution of the expansion velocity $v_{\text{exp}}(t)$, of pair correlations and of entanglement, (b) the change of the dynamics with the system dimensionality D , (c) the momentum distribution of the expanding correlated fermions, and (d) the approach of the thermodynamic limit, $N \rightarrow \infty$. Here, a striking universal behavior is discovered: for all U and D , the expansion velocity decreases with system size according to $v_{\text{exp}}^{\infty}(N) - V_{\text{exp}} \sim N^{-1/2}$, where we denoted the long-time asymptotics by $v_{\text{exp}}^{\infty} \equiv v_{\text{exp}}(t \rightarrow \infty)$ and $V_{\text{exp}} \equiv v_{\text{exp}}^{\infty}(N \rightarrow \infty)$.

This paper is organized as follows. In Sec. II, we introduce the D -dimensional Hubbard model and summarize the basic formulas of the nonequilibrium Green functions approach. In Sec. III, we present the numerical results. In Sec. IV, we conclude with a summary and a discussion of our results.

II. THEORY**A. Hubbard model**

We consider the D -dimensional Hubbard model with N_s sites that are labeled by a D -dimensional index $s =$

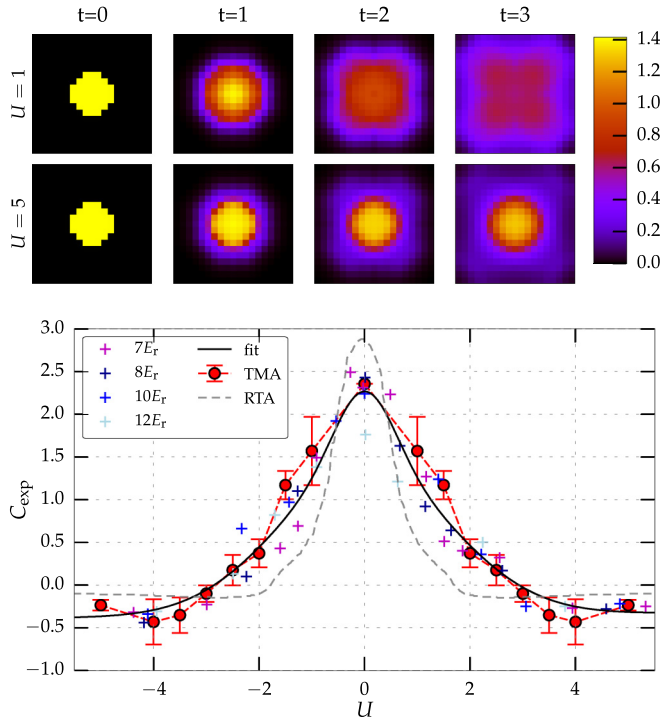


FIG. 1. (Top) Expansion dynamics of 74 circularly confined fermions in a 2D 19×19 Hubbard lattice (1) following the removal of the confinement at time $t = 0$, for $U = 1(5)$, first (second) row. Snapshots of the density n_s for four time points during the early stage of the expansion (t in units of the inverse hopping rate, color code: $\sqrt{n_s}$). (Bottom) Asymptotic core [defined as density HWHM] expansion velocity C_{exp} . Plus signs: experimental results for different lattice depths in units of the recoil energy E_r [10]; gray dashed line: RTA model [4]; red circles: present NEGF results. The black line is a fit through the experimental points to guide the eye.

(s_1, \dots, s_D) and the local spin projection is denoted by $\sigma \in \{\uparrow, \downarrow\}$. The Hamiltonian is, in second quantization, expressed in terms of creation and annihilation operators $\hat{c}_{s,\sigma}^\dagger$ and $\hat{c}_{s,\sigma}$:

$$H(t) = - \sum_{\langle s,s' \rangle} \sum_{\sigma=\uparrow,\downarrow} \hat{c}_{s,\sigma}^\dagger \hat{c}_{s',\sigma} + U \sum_s \hat{c}_{s,\uparrow}^\dagger \hat{c}_{s,\uparrow} \hat{c}_{s,\downarrow}^\dagger \hat{c}_{s,\downarrow} + \sum_s \sum_{\sigma=\uparrow,\downarrow} V_s^R(t) \hat{c}_{s,\sigma}^\dagger \hat{c}_{s,\sigma}, \quad (1)$$

and, in the first (hopping) term, $\langle s,s' \rangle$ denotes nearest-neighbor sites. The second term describes on-site interactions of electrons with opposite spin, which has the strength U . In the third term, $V_s^R(t)$ is a circular potential of radius R that initially confines N fermions occupying $N/2$ sites in the trap center. In the present paper, we consider the dynamics that are initiated by a potential quench, i.e., at time $t = 0$, V^R is switched off what initiates a diffusion process, as, e.g., in the experiment [4].

B. Nonequilibrium Green functions

Our goal is to study the correlated expansion dynamics of spatially inhomogeneous finite Hubbard clusters with a single-site resolution. We are interested in the dynamics on all time scales while exactly fulfilling the many-particle conservation

laws of particle number, momentum, and total energy. This can be achieved using NEGF that are defined on the Keldysh time contour \mathcal{C} with the contour-time-ordering operator $T_{\mathcal{C}}$ as

$$G_{ss'}^\sigma(z, z') = -\frac{i}{\hbar} \langle T_{\mathcal{C}} \hat{c}_{s,\sigma}(z) \hat{c}_{s',\sigma}^\dagger(z') \rangle. \quad (2)$$

The Green functions can be understood as generalized time-dependent single-particle density matrices on the lattice where the presence of two time arguments allows to incorporate spectral information, and $\langle \dots \rangle$ denotes the ensemble average. The equations of motion for the NEGF are the Keldysh–Kadanoff–Baym equations (KBE) [21,22],

$$\left(i\hbar \frac{\partial}{\partial z} \delta_{s,\bar{s}} - h_{s\bar{s}}^\sigma \right) G_{s\bar{s}'}^\sigma(z, z') = \delta_{\mathcal{C}}(z - z') \delta_{s,s'} + \int_{\mathcal{C}} d\bar{z} \Sigma_{s\bar{s}}^\sigma(z, \bar{z}) G_{\bar{s}s'}^\sigma(\bar{z}, z'), \quad (3)$$

and its adjoint (summation over \bar{s} is implied). In order to account for correlation effects in the dynamics, the self-energy Σ includes, in addition to mean-field (Hartree-Fock), also correlation contributions. For weak to moderate coupling ($|U| \lesssim 1$), the second-order Born approximation is appropriate [23], which includes all irreducible diagrams of second order in the interaction (second order in U). However, for the case of strong correlations (large $|U|$), the next orders (third, fourth powers of U) become comparable and perturbation theory fails. Therefore one has to sum up the entire Born series, i.e., diagrams of all orders in U . This is equivalent to the T -matrix approximation to the correlation self-energy (TMA [24]), which reads, for the Hubbard model [25],

$$\Sigma_{ss'}^{\text{cor},\uparrow(\downarrow)}(z, z') = i\hbar T_{ss'}(z, z') G_{s's}^{\downarrow(\uparrow)}(z', z), \quad (4)$$

$$T_{ss'}(z, z') = -i\hbar U^2 G_{ss'}^\uparrow(z, z') G_{ss'}^\downarrow(z, z') + i\hbar U \int_{\mathcal{C}} d\bar{z} G_{s\bar{s}}^\uparrow(z, \bar{z}) G_{\bar{s}s'}^\downarrow(\bar{z}, z') T_{s\bar{s}}(\bar{z}, z'). \quad (5)$$

Here, T can be understood as an effective interaction obeying the Lippmann-Schwinger equation (5), e.g., Refs. [20,22,27]. The first term in (5) alone describes the interaction of a single fermion pair and corresponds to the second-order Born approximation, whereas the integral term adds interaction contributions of all orders (in U).

We underline the conserving character of this approximation [22] and, in fact, conservation of particle number and *total energy* is observed to high accuracy in all our simulations. Further, time-reversal symmetry is guaranteed (as it should be since the system is isolated). Also, our simulations yield the same time-dependent densities when U is replaced by $-U$ confirming the dynamical symmetry demonstrated in Refs. [4,28].

The two-time KBE have been solved for a variety of spatially homogeneous systems, including dense plasmas and optically excited semiconductors [29–31] or the uniform electron gas [32]. More recently, spatially inhomogeneous systems were studied, in particular, the ionization dynamics of few-electron atoms [33–35] and quantum dots [2]. All these simulations used self-energies on the level of the static second Born approximation. Only recently the use of the two-time TMA, under full nonequilibrium conditions, has

become possible for the Hubbard model in Refs. [23,25,36]. However, only very small 1D systems ($N \leq 6, U \leq 4$) could be simulated for rather short times. Here, we report a dramatic extension of TMA simulations in terms of particle number, simulation duration, and dimensionality. With this, it is possible, for the first time, to access experimentally relevant situations. We systematically study up to $N = N^\uparrow + N^\downarrow = 2N^\uparrow = 114$ fermions in a broad range of coupling parameters, $0 \leq |U| \leq 8$, in a one-, two-, and three-dimensional lattice.

III. RESULTS

The initial state of our simulations is a doubly occupied spherical central region in the ground state [4] that is confined by a properly chosen potential V^R which is turned off at $t = 0$. In our simulations we use a steplike potential. We show in Sec. III E that the precise functional form has a negligible effect on the expansion dynamics. The KBE (3) are then solved with this initial condition for the two-time correlation function $G_{ss'}^{\sigma,\prec}(t,t')$ (the less component of the NEGF (2)[21,37]) yielding the time dependence of all observables.

Figure 1 shows snapshots of the site-resolved particle density $n_s(t) = n_s^\uparrow(t) + n_s^\downarrow(t)$ with $n_s^\sigma(t) = -iG_{ss}^{\sigma,\prec}(t,t)$, for two couplings, $U = 1, 5$. For $U = 1$, the density rapidly evolves towards the square symmetry of the lattice, whereas for $U = 5$ the core region remains circular over the entire simulation duration, in agreement with experimental observations [4].

A. Time evolution of the expansion velocity

The density evolution is quantified by the diameter $d(t) = \sqrt{R^2(t) - R^2(0)}$, corrected for its starting value $R(0)$,

$$R^2(t) = \frac{1}{N} \sum_s^{N_s} n_s(t) \|s - s_0\|^2, \quad s_0 = \frac{1}{N} \sum_s^{N_s} n_s(0) s,$$

where the center of mass s_0 is immobile in the present case. The left part of Fig. 2 shows the dynamics of the instantaneous expansion velocity

$$v_{\text{exp}}(t) = \frac{d}{dt}d(t), \quad (6)$$

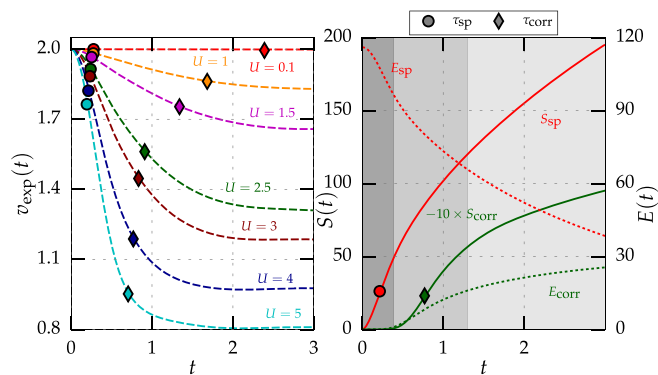


FIG. 2. (Left) Time evolution of the expansion velocity for $N = 58$ in 2D and various U . (Right) Evolution of the independent-particle and correlation parts of the entropy and energy, for $U = 4$. Symbols mark the respective inflection points. Shaded areas correspond to the three phases of the evolution (see text).

for various U , for a typical case, $N = 58$ in 2D. As the system is initially uncorrelated, the expansion starts ballistically from the ideal value, $v_{\text{exp}}(0) = v^{\text{id}} = \sqrt{2D} = 2$, and converges to a smaller asymptotic value, v_{exp}^∞ . These asymptotics monotonically decrease with increasing coupling strength U . This trend is well known and easily understood: the diffusion front forms at the cluster edge since particles in the “bulk” cannot move due to the Pauli principle, since all neighboring lattice sites are occupied. When $|U|$ grows, the expansion of the outermost particles is slowed down due to the growing interaction with the bulk particles. Here, we can quantify this trend, for the first time, for two- and three-dimensional systems.

B. Short-time dynamics. Build-up of correlations and entanglement

The time evolution of $v_{\text{exp}}(t)$ is not trivial and results from the interplay between independent-particle and correlation effects. To quantify this, we decompose the double occupation [38] of each site s into a factorized part (“fac”) and a correlation part (“corr,” the reminder)

$$n_s^{\uparrow\downarrow} = \langle \hat{c}_{s,\uparrow}^\dagger \hat{c}_{s,\uparrow} \hat{c}_{s,\downarrow}^\dagger \hat{c}_{s,\downarrow} \rangle =: n_s^{\uparrow\downarrow,\text{fac}} + n_s^{\uparrow\downarrow,\text{corr}}, \quad (7)$$

$$n_s^{\uparrow\downarrow,\text{fac}} = n_s^\uparrow n_s^\downarrow. \quad (8)$$

The factorized contribution is formally equivalent to the contribution of independent particles. Note, however, that the single-particle densities entering $n_s^{\uparrow\downarrow,\text{fac}}$ are obtained from a fully correlated calculation and, thus, the factorized term also contains interaction effects.

With this, we identify the corresponding components of the energy ($E_{\text{fac}}, E_{\text{corr}}$) [23] as well as the entanglement entropy [38,39],

$$S = S_{\text{fac}} + S_{\text{corr}} = \sum_s S_s, \quad (9)$$

$$S_s = -2 \left(\frac{n_s}{2} - n_s^{\uparrow\downarrow} \right) \log_2 \left(\frac{n_s}{2} - n_s^{\uparrow\downarrow} \right) - n_s^{\uparrow\downarrow} \log_2 n_s^{\uparrow\downarrow} - (1 - n_s + n_s^{\uparrow\downarrow}) \log_2 (1 - n_s + n_s^{\uparrow\downarrow}). \quad (10)$$

Here, the factorized contribution, S_{fac} follows from the total entropy by the replacement Eq. (8).

The dynamics of these two energy and entropy contributions are dominated by single-particle and correlation effects, respectively, and it is well known from the dynamics of uniform systems [21,29,40] that they proceed on rather different time scales: typically pair correlations relax substantially faster than single-particle quantities. In the expansion dynamics of the present Hubbard clusters we also observe a sequence of time scales, however, the details are very different. We identify three characteristic phases: during the *first phase*, S_{fac} (E_{fac}) is being built up (destroyed), resulting in a decrease of v_{exp} , see Fig. 2. Here, the increase of S_{fac} measures the transition from a state of independent particles ($S = 0$) to an interacting many-body state. The inflection point τ_{fac} (circles) of S_{fac} (and E_{fac}) is representative for the time scale of this phase. The *second phase* is characterized by the saturation of E_{fac} and v_{exp} . The simultaneous build-up of correlations partly prolongs

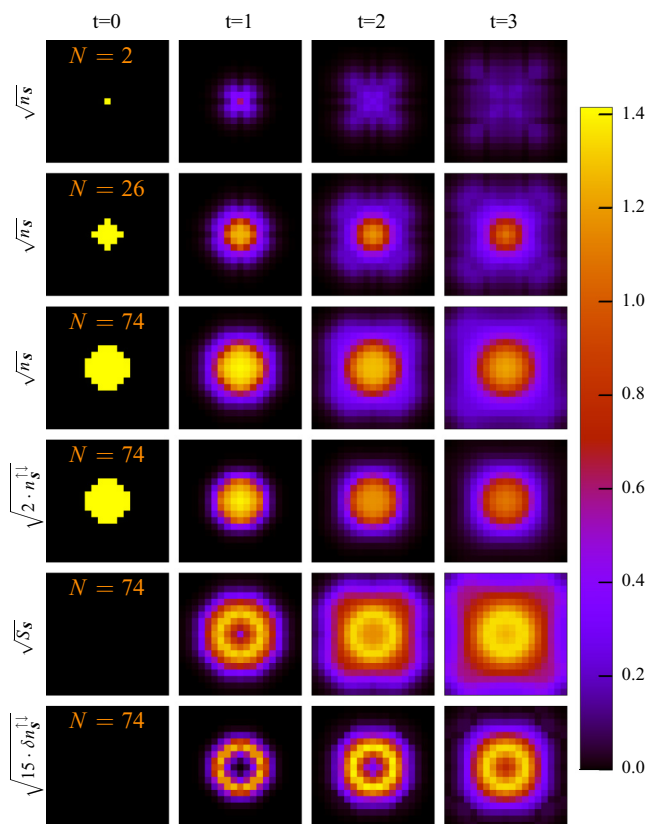


FIG. 3. Fermion expansion dynamics in a 2D 19×19 Hubbard lattice (1) at $U = 4$. Top three rows: square root of density n_s for $N = 2, 26$, and 74 , respectively. Rows 4–6: square root of double occupation, entropy density S_s , and the pair correlation function $\delta n_s^{\uparrow\downarrow} = n_s^{\uparrow\downarrow} - n_s^{\uparrow} n_s^{\downarrow}$.

the saturation and determines the final value, v_{exp}^{∞} . The time scale of these processes is the correlation time τ_{corr} [21,40], which is estimated by the inflection point of S_{corr} (and E_{corr} , diamonds). Both phases become shorter when U is increased, i.e., correlations accelerate the early dynamics, cf. left part of Fig. 2. It is evident that τ_{corr} is one order of magnitude larger than τ_{fac} —in striking contrast to homogeneous systems as discussed above. The main difference here is the strong inhomogeneity leading to a spatially localized formation of correlations and entanglement [see Sec. III C] and the formation of a diffusion front.

C. Single-site resolved expansion and correlation dynamics

Additional insight into the physics is gained from a site-resolved analysis which is presented in Fig. 3. The top three rows show the dynamics in 2D for a fixed U and three particle numbers. Quantum interference effects are evident for small N . Further, the dynamics are slowing down with increasing N , because only fermions at the cluster edge are mobile, in the beginning, due to the Pauli principle. The fourth row displays the spatial distribution of the double occupation $n_s^{\uparrow\downarrow}$. It originally coincides with the single-particle density (third row) but then the two decouple. The much slower doublon expansion is the first indication of “quantum distillation”[41] of fermions in 2D. Finally, the emergence of entanglement and

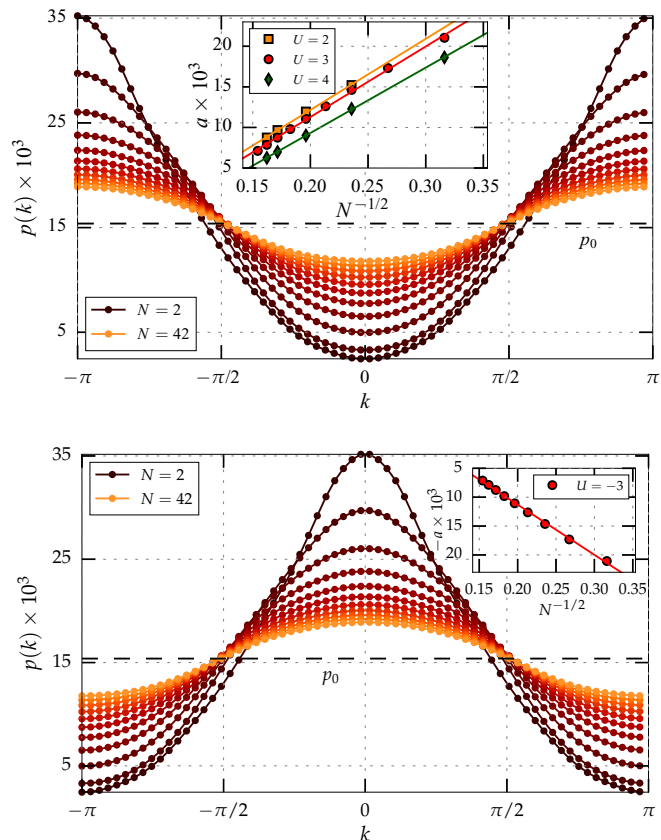


FIG. 4. Momentum distribution $p(k)$, Eq. (11) at $t = 9.5$, for a 1D system of $N_s = 65$ for $N = 2, \dots, 42$. (Top) $U = 3$. (Bottom) $U = -3$. The dashed lines denotes the uniform initial distribution $p_0(k)$. (Insets) N -dependence of amplitude a . Symbols: data points, lines: linear fits.

of pair correlations is shown in rows 5 and 6. Both start from zero everywhere and emerge first at the cluster boundary from where they propagate inward and outward. These processes are accelerated (slowed down) with increasing U (N), which explains the corresponding behavior of the characteristic time scales τ_{fac} and τ_{corr} .

D. Hydrodynamic expansion phase. Momentum distribution

The *third and final phase* is the hydrodynamic expansion where v_{exp} , the correlations and the momentum distribution have become stationary, see Fig. 4, whereas the independent-particle energy and entropy continue to evolve, cf. Fig. 2. Figure 4 shows the normalized momentum distribution, $p(\mathbf{k}) = n(\mathbf{k})/N$ [obtained from the site occupations], of a 1D system for $U = 3$ at the end of the simulation. For all N , $p(\mathbf{k})$ is oscillatory with an amplitude a that monotonically decreases with N . For large N , it is very well described by the function

$$p(\mathbf{k}) = p(k) = N_s^{-1} - a \cos(k), \quad (11)$$

where the value of $a(U, N)$ is shown in the inset of Fig. 4 for different U . It is obvious that, for positive U , $p(k)$ is peaked at $\pm\pi$ while the maximum of the occupation is around $k = 0$, for negative U . We note that these results are in agreement with the qualitative predictions in Ref. [28]. A striking observation is

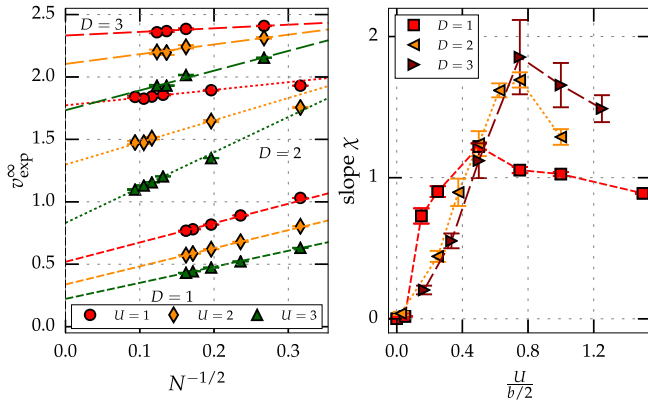


FIG. 5. (Left) Asymptotic expansion velocity vs particle number for $D = 1, \dots, 3$ and $U = 1, \dots, 3$. Symbols correspond to data points, errors are smaller than symbol size. Dashed lines: linear extrapolation $N \rightarrow \infty$ according to Eq. (13). (Right) Corresponding slope χ vs bandwidth-normalized interaction.

the particle number dependence of the momentum distribution. We observe that the amplitude of the oscillations scales as $a \sim N^{-1/2}$. The origin of this scaling is presently an open question but this behavior was observed in all cases and appears to be universal.

To quantify the stationary hydrodynamic expansion we extrapolate the expansion velocity to $t \rightarrow \infty$, denoting the result by v_{exp}^{∞} . It is obtained from $v_{\text{exp}}(t)$ by averaging over all times exceeding t_{avg} where saturation is reached (cf. Fig. 2) and which is given by

$$\left| \frac{1}{v_{\text{exp}}(t)} \frac{dv_{\text{exp}}(t)}{dt} \right| < \epsilon, \quad (12)$$

for all $t > t_{\text{avg}}$ and a given small parameter ($\epsilon \ll 1$). To quantify the error of v_{exp}^{∞} , we use the standard deviation $\sigma(v_{\text{exp}}^{\infty})$ of the averaging process.

An interesting question is how the expansion of a group of N fermions depends on the value of N and the system dimensionality D . The results of the extrapolation are shown in the left part of Fig. 5. Again, we observe a monotonic decrease with U and, furthermore, a systematic increase of v_{exp}^{∞} with D , that is due to the enlarged number of degrees of freedom.

E. Influence of particle number and dimensionality. Extrapolation to the macroscopic limit

The most striking observation is the N dependence of v_{exp}^{∞} and its approach to the macroscopic limit: for any fixed U and D and sufficiently large N , we observe the scaling

$$v_{\text{exp}}^{\infty}(U; N; D) - V_{\text{exp}}(U; D) = \chi(U; D)N^{-1/2}, \quad (13)$$

$$V_{\text{exp}}(U; D) \equiv \lim_{N \rightarrow \infty} v_{\text{exp}}^{\infty}(U; N; D). \quad (14)$$

Interestingly, this N dependence is the same as in the momentum distribution (11), cf. Fig. 4 and is caused by the latter.

For the extrapolation, V_{exp} and the slope χ are used as fit parameters. Only particle numbers N larger than a cutoff value

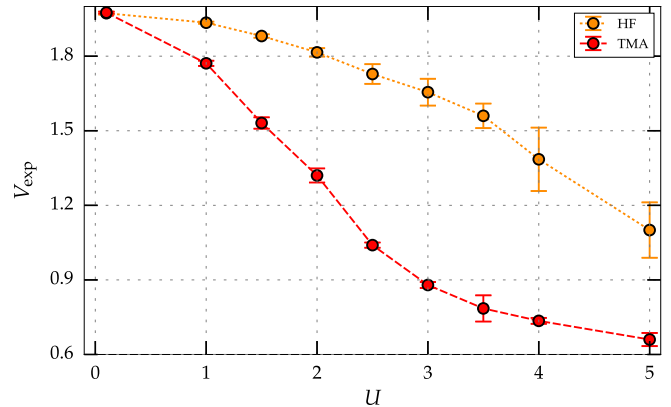


FIG. 6. Macroscopic expansion velocity V_{exp} for varying U . Comparison between Hartree-Fock (HF) and the correlated T -matrix (TMA) results.

N^* are taken into account. The errors $\sigma(v_{\text{exp}}^{\infty})$ are also included in the fit process, resulting in the final statistical uncertainty, $\sigma(V_{\text{exp}})$. We note that our procedure is very similar to the one applied for the diffusion of a Mott insulator and Néel state in a 1D fermionic system in Ref. [42].

The right-hand part of Fig. 5 shows the dependency of the slope χ on the bandwidth-normalized interaction strength $U/(b/2)$ with the effective bandwidth $b = 4D$. For all D and N , χ starts from zero, at $U = 0$, which is a consequence of ballistic expansion of noninteracting particles. When U is increased further, χ reaches a maximum slightly below $U = (b/2)$ and then decreases again. The reason for the latter is that fermions on doubly occupied sites are effectively frozen, at large U , regardless of N . In-between these two limits, the slope shows a qualitatively similar behavior for all D : a steep rise (slow decrease) for small (large) U .

We now turn to the analysis of the macroscopic limit of the expansion velocity, V_{exp} . In Fig. 6, we show V_{exp} as a function of U and confirm the monotonic reduction that was observed before for finite N , cf. Fig. 2. The error bars show the total statistical error resulting from the time averaging and the extrapolation with respect to N . We also show, for comparison, the Hartree-Fock approximation, which exhibits strong deviations, which underlines the key role of correlations in the present quench dynamics.

Similar to our procedure of obtaining the asymptotic expansion velocity v_{exp}^{∞} and its macroscopic limit, we can proceed with the core expansion velocity c_{exp}^{∞} and its macroscopic limit, C_{exp} . The experimental results of Schneider *et al.* [4] for a 2D Hubbard system and our T -matrix results were displayed in Sec. I, in Fig. 1. We now explain how our results were obtained. For the case $D = 2$, the density distribution is averaged azimuthally for each time step. The half width at half maximum of the resulting density profile, $R_{\text{HWHM}}(t)$, is used to measure the “core” width. Adjusted for the initial core width, R_{HWHM}^0 , c_{exp}^{∞} is determined by fitting the resulting $R_{\text{HWHM}}(t)$ to

$$R_{\text{HWHM}}(t) = \sqrt{(R_{\text{HWHM}}^0)^2 + (c_{\text{exp}}^{\infty} t)^2} \quad (15)$$

for all $t > t_{\text{avg}}$ with R_{HWHM}^0 and c_{exp}^{∞} as free fitting parameters. Since the core of the density distribution starts to shrink for

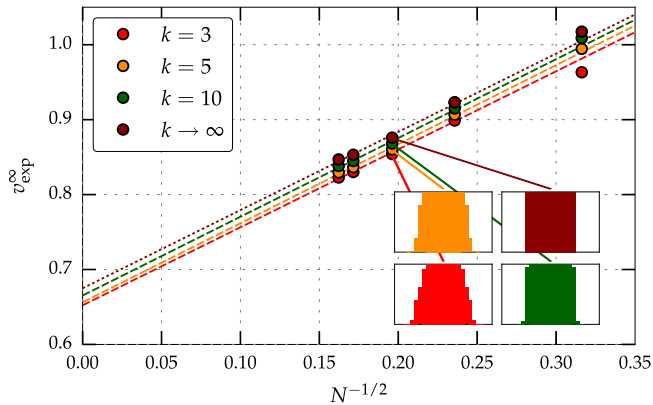


FIG. 7. Dependence of the asymptotic expansion velocity on N for confinement potentials of different curvature $\gamma_k(N)$. Insets show the shape of the initial density profile.

sufficiently large interaction strength U , we apply

$$R_{\text{HWHM}}(t) = \sqrt{(R_{\text{HWHM}}^0)^2 - (c_{\text{exp}}^\infty t)^2} \quad (16)$$

instead, following Ref. [4], and consider c_{exp}^∞ the speed of contraction of the core region.

The extrapolation of c_{exp}^∞ is done as in Eq. (13), resulting in the macroscopic core expansion velocity C_{exp} , confirming the scaling with $N^{-1/2}$. This robust scaling with N allows us to perform the thermodynamic limit, $N \rightarrow \infty$. This yields the results that were presented in Fig. 1, and that exhibit excellent agreement with the experiment over the entire U range, including the zero crossing of C_{exp} around $U = 3$.

One may wonder whether the results depend on the chosen steep confinement, cf. Figs. 1 and 3. Here, we demonstrate that the shape of the initial confinement has only a minor effect on the asymptotic expansion velocity, in agreement with the observations in Ref. [43]. To this end, we use a harmonic confinement

$$V(R) = \gamma_k R^2, \quad (17)$$

with curvature γ_k . To achieve a similar shape for different N , we choose

$$\gamma_k(N) = k/N, \quad (18)$$

for three strengths $k = 3, 5, 10$. Together with the steplike potential ($k \rightarrow \infty$), the results are shown in Fig. 7. Even though the initial density profile is affected by the curvature (see inset), the expansion velocity is not. In particular, the macroscopic limit, V_{exp} changes by less than 10%.

IV. DISCUSSION

To summarize, we have introduced T -matrix NEGF simulations into the field of fermion dynamics in Hubbard lattices providing the first accurate quantum dynamics results [24] for two and three dimensions [44]. While the magnitude of the error of NEGF simulations with T -matrix self-energies for the present large systems is not exactly known, for the cases where the exact results are available (small N , 1D) the agreement is excellent [23,25,26]. It is expected that the accuracy will further improve when N increases, as well as in higher dimensions. The largest uncertainty is expected for Hubbard clusters at half-filling and for small integrable systems. Further tests are needed to verify and quantify this behavior.

Our results for 2D fermionic Hubbard clusters exhibit excellent quantitative agreement with recent experiments that investigated the final stage of the expansion dynamics following a confinement quench [4]. They, moreover, yield detailed information on the early stages of the dynamics of correlated fermions, including the buildup and propagation of correlations and entanglement and on the effect of the system dimensionality. Furthermore, we uncovered a universal scaling of macroscopic quantities with N . Our predictions, including the site-resolved results for the pair correlations and entanglement entropy, can be directly tested experimentally using the novel quantum-gas microscopes [15–17].

ACKNOWLEDGMENTS

We acknowledge discussions with L. Oesinghaus during the early stage of this work as well as helpful comments by F. Heidrich-Meisner (Munich). This work is supported by the Deutsche Forschungsgemeinschaft via Grant BO1366/9 and by Grant SHP0013 for super-computing time at the HLRN.

-
- [1] *The LDA+DMFT Approach to Strongly Correlated Materials*, edited by E. Pavarini, E. Koch, D. Vollhardt and A. Lichtenstein (Forschungszentrum Jülich GmbH, Zentralbibliothek, Verlag 2011).
- [2] K. Balzer, M. Bonitz, R. van Leeuwen, A. Stan, and N. E. Dahlen, *Phys. Rev. B* **79**, 245306 (2009).
- [3] A.-M. Uimonen, E. Khosravi, A. Stan, G. Stefanucci, S. Kurth and R. van Leeuwen, and E. K. U. Gross, *Phys. Rev. B* **84**, 115103 (2011).
- [4] U. Schneider, L. Hackermüller, J. P. Ronzheimer, S. Will, S. Braun, T. Best, I. Bloch, E. Demler, S. Mandt, D. Rasch, A. Rosch, *Nat. Phys.* **8**, 213 (2012).
- [5] J. Kajala, F. Massel, and P. Törmä, *Phys. Rev. Lett.* **106**, 206401 (2011).
- [6] J. P. Ronzheimer, M. Schreiber, S. Braun, S. S. Hodgman, S. Langer, I. P. McCulloch, F. Heidrich-Meisner, I. Bloch, and U. Schneider, *Phys. Rev. Lett.* **110**, 205301 (2013).
- [7] L. Vidmar, J. P. Ronzheimer, M. Schreiber, S. Braun, S. S. Hodgman, S. Langer, F. Heidrich-Meisner, I. Bloch, and U. Schneider, *Phys. Rev. Lett.* **115**, 175301 (2015).
- [8] L. Xia, L. A. Zundel, J. Carrasquilla, A. Reinhard, J. M. Wilson, M. Rigol, and D. S. Weiss, *Nat. Phys.* **11**, 316 (2015).
- [9] H. D. Whitley, Ch. R. Scullard, L. X. Benedict, J. I. Castor, A. Randles, J. N. Glosli, D. F. Richards, M. P. Desjarlais, and F. R. Graziani, *Contrib. Plasma Phys.* **55**, 192 (2015).
- [10] We include all values E_r shown in Ref. [4] in the comparison.

- [11] S. Trotzky, Y.-A. Chen, A. Flesch, I. P. McCulloch, U. Schollwöck, J. Eisert, and I. Bloch, *Nature (London)* **8**, 484 (2012).
- [12] M. Cheneau, P. Barmettler, D. Poletti, M. Endres, P. Schauß, T. Fukuhara, C. Gross, I. Bloch, C. Kollath, and S. Kuhr, *Nature (London)* **481**, 484 (2012).
- [13] S. Will, D. Iyer, and M. Rigol, *Nat. Comm.* **6**, 6009 (2015).
- [14] X. Zhang, C.-L. Hung, S.-K. Tung, and C. Chin, *Science* **335**, 1070 (2012).
- [15] L. W. Cheuk, M. A. Nichols, M. Okan, T. Gersdorf, V. V. Ramasesh, W. S. Bakr, T. Lompe, and M. W. Zwierlein, *Phys. Rev. Lett.* **114**, 193001 (2015).
- [16] M. F. Parsons, F. Huber, A. Mazurenko, C. S. Chiu, W. Setiawan, K. Wooley-Brown, S. Blatt, and M. Greiner, *Phys. Rev. Lett.* **114**, 213002 (2015).
- [17] E. Haller *et al.*, *Nat. Phys.* **11**, 738 (2015).
- [18] For completeness, we mention recent simulations of the expansion dynamics in 3D Hubbard systems with time-dependent DFT [19]. However, they used the adiabatic local density approximation, the reliability of which is still under debate, and considered coupling strengths which are larger than the ones studied in Ref. [4].
- [19] A. Kartsev, D. Karlsson, A. Privitera, and C. Verdozzi, *Sci. Rep.* **3**, 2570 (2013).
- [20] D. Kremp, M. Bonitz, W. D. Kraeft, and M. Schlanges, *Ann. Phys. (N. Y.)* **258**, 320 (1997).
- [21] M. Bonitz, *Quantum Kinetic Theory*, 1st ed. (B. G. Teubner, Leipzig, Germany, 1998); *Quantum Kinetic Theory*, 2nd ed. (Springer International Publishing, Cham, Switzerland, 2015).
- [22] L. P. Kadanoff and G. Baym, *Quantum Statistical Mechanics* (Benjamin, New York, 1962).
- [23] S. Hermanns, N. Schlünzen, and M. Bonitz, *Phys. Rev. B* **90**, 125111 (2014).
- [24] The T -matrix approximation shows very good agreement with exact diagonalization results where available (small N) [23, 25, 26]. Since it is a low-density approximation, small systematic errors are expected around half-filling.
- [25] M. Puig von Friesen, C. Verdozzi and C.-O. Almbladh, *Phys. Rev. Lett.* **103**, 176404 (2009).
- [26] M. Puig von Friesen, C. Verdozzi and C.-O. Almbladh, *Phys. Rev. B* **82**, 155108 (2010).
- [27] D. Semkat, D. Kremp, and M. Bonitz, *J. Math. Phys.* **41**, 7458 (2000).
- [28] U. Schneider, Ph.D. Dissertation, University Mainz, 2010.
- [29] M. Bonitz, D. Kremp, D. C. Scott, R. Binder, W. D. Kraeft, and H. S. Köhler, *J. Phys. Condens. Matter* **8**, 6057 (1996).
- [30] R. Binder, H. S. Köhler, M. Bonitz, and N. Kwong, *Phys. Rev. B* **55**, 5110 (1997).
- [31] N. H. Kwong, M. Bonitz, R. Binder and S. Köhler, *Phys. Stat. Sol.* **206**, 197 (1998).
- [32] N. H. Kwong, and M. Bonitz, *Phys. Rev. Lett.* **84**, 1768 (2000).
- [33] N. E. Dahlen, and R. van Leeuwen, *Phys. Rev. Lett.* **98**, 153004 (2007).
- [34] K. Balzer, S. Bauch, and M. Bonitz, *Phys. Rev. A* **81**, 022510 (2010).
- [35] K. Balzer, S. Bauch, and M. Bonitz, *Phys. Rev. A* **82**, 033427 (2010).
- [36] M. Bonitz, S. Hermanns, and N. Schlünzen, *Contrib. Plasma Phys.* **55**, 152 (2015).
- [37] G. Stefanucci and R. van Leeuwen, *Nonequilibrium Many-Body Theory of Quantum Systems* (Cambridge University Press, Cambridge UK, 2031).
- [38] M. Puig von Friesen, C. Verdozzi and C.-O. Almbladh, *Europ. Phys. Lett.* **95**, 27005 (2011).
- [39] D. Larsson and H. Johannesson, *Phys. Rev. Lett.* **95**, 196406 (2005).
- [40] M. Bonitz, and D. Kremp, *Phys. Lett. A* **212**, 83 (1996); M. Bonitz, *ibid.* **221**, 85 (1996).
- [41] F. Heidrich-Meisner, S. R. Manmana, M. Rigol, A. Muramatsu, A. E. Feiguin, and E. Dagotto, *Phys. Rev. A* **80**, 041603 (2009).
- [42] L. Vidmar, S. Langer, I. P. McCulloch, U. Schneider, U. Schollwöck, and F. Heidrich-Meisner, *Phys. Rev. B* **88**, 235117 (2013).
- [43] S. Langer, M. J. A. Schuetz, I. P. McCulloch, U. Schollwöck, and F. Heidrich-Meisner, *Phys. Rev. A* **85**, 043618 (2012).
- [44] For more details, see N. Schlünzen, and M. Bonitz, *Contrib. Plasma Phys.* **56** (to be published in 2016).